Chapter 4

Role of Bimetallic Catalysts in Steam Methane Reforming

4.1 Introduction

It is reported in the literature that noble metals showed outstanding catalytic performance for SRM which includes ruthenium, rhodium, and platinum. [1] They gave superior activity, stability, resistance to carbon deposition, and fast response time, especially rhodium. [2-3] However, the high cost of noble metals makes their usage uneconomical. Consequently, more attention was made on the use of less expensive transition metal catalysts such as Ni and Co. [4] Industrially, Ni based catalysts are the most widely used. [5–8] However, deactivation via the sintering process and high rate of coke deposition, particularly at high temperatures, and higher CO selectivity are the major concerns with the Ni based catalyst. [9]

The coke deposition in Ni based catalysts can be minimized by reducing the formation of nickel carbide due to alloy segregation, through the gasification or oxidation of deposited coke. [10] High water adsorption and/or higher oxygen mobility can result in minimizing the coke formation by enhancing the gasification or oxidation of deposited coke. The pristine surface of alumina adsorbs the water which initiates the carbon gasification reaction and reduces the coke deposition while Ceria mobilizes the lattice oxygen which oxidize the deposited coke. Hence, alumina and ceria supports are widely used in the literature for the SMR process. In this work, we have used alumina and ceria as a support material. In literature, many authors have used promoters to enhance the catalytic activity of the Ni. [11] However, the effect of La and Fe as a promotor on Ni based catalysts is not investigated throughly. According to Lucredio et al. [12] Ni with La as a promoter results in strong catalytic activity at low temperatures and significantly lower carbon production

in partial oxidation of methane reactions. [13] Fatesh et al. [14] reported that Ni on lanthanum oxide (La_2O_3) increases the catalytic activity in the dry reforming of methane. [15] The addition of lanthanum improves metallic dispersion and has positive effects on active phase support interaction, sintering resistance, and carbon deposition. [16] Similarly, Fe improves the WGS reaction performance and hence helps in reducing the CO selectivity. [17] Therefore, in the current work, La and Fe promoted Ni based catalyst is synthesized for steam reforming of methane targeting membrane reformer application. The study uses commercial alumina and ceria as support. Further, the complete characterization of the catalyst is performed using XRD, BET, and SEM/EDS. Finally, the performance of the synthesized catalyst is tested in a packed bed reactor in terms of conversion, H_2 yield, CO, and CO_2 selectivity. The experiments are performed for different operating conditions to find the optimal operating condition for each catalyst. The newly synthesized catalyst provides low temperature operation, and lower CO selectivity, which makes it suitable for the 'on-site' generation of hydrogen through a membrane reformer.

4.2 Experimental analysis

4.2.1 Materials

Commercial γ- Al_2O_3 and ceria of Sigma –Aldrich was used as a precursor for the support. The nickel nitrate hexahydrate ($Ni(NO_3)_2.6H_2O$), lanthanum nitrate hexahydrate ($La(NO_3)_3.6\ H_2O$) and ferric nitrate nonahydrate ($Fe(NO_3)_3.9H_2O$) were also obtained from Sigma-Aldrich (Purity > 99 %).

4.2.2 Catalyst Synthesis

The γ- Al_2O_3 was thermally treated at a controlled rate in a programable tube furnace to obtain θ- Al_2O_3 which was used as a support while commercial ceria was directly used. Six different catalysts were synthesized by changing the support, and doped metals which were:

Ni/Al_2O_3, $Ni\text{-}La/Al_2O_3$, $Ni\text{-}Fe/Al_2O_3$ using θ- Al_2O_3 as support, and Ni/CeO_2, $Ni\text{-}La/CeO_2$, and $Ni\text{-}Fe/CeO_2$ using ceria as support. The results are compared with monometallic catalysts (Ni/Al_2O_3, Ni/CeO_2) to find the effect of each promotor on the catalyst performance. All the catalysts were synthesized using wet impregnation method with a total metal loading of 10 % at distinct Ni-La and Ni-Fe scales of 3/1, respectively.

The 10 wt % metal loading was selected as it is reported as optimum metal loading in the literature on steam methane reforming. [23] A mixed aqueous solution of $Ni(NO_3)_2.6H_2O$ and $Fe(NO_3)_3.9H_2O$ salts at Ni/Fe scale 1/3 was impregnated on both the supports. The mixtures were agitated for 6 hours at 70 °C. Then the samples were dried in an air oven overnight at 120 °C and calcined at 970 °C in Nabotherm tube furnace. The resulting materials were palletized, crushed, and sieved to a size range of 180– 300 microns. The composition of different prepared catalyst is tabulated in Table 4.1.

Table 4.1. Composition of prepared catalysts.

Catalyst	Ni Metal load (%)	La Metal load (%)	Fe Metal load (%)
10 % Ni/ Al_2O_3	10	0	0
10 % Ni-La/Al_2O_3	7.5	2.5	0
10 % Ni-Fe/Al_2O_3	7.5	0	2.5
10 % Ni/CeO_2	10	0	0
10 % Ni-La/CeO_2	7.5	2.5	0
10 % Ni-Fe/CeO_2	7.5	0	2.5

4.2.3 Catalyst Characterization

To ascertain the physical and chemical characteristics of the prepared catalysts, some of the catalysts were examined using SEM (Scanning Electron Microscope), XRD (X-Ray Diffraction), and BET (Brunauer-Emmett-Teller) surface area analyzer.

X-ray diffraction (XRD) patterns of samples were recorded on (Rigaku XRD analyzer) using Cu Kα (= 0.154 nm) radiation in the 2θ range of 10–90 degrees. The catalyst phases were identified by comparing the collected spectra to those in the JCPDS data set (Joint Committee of powder diffraction standards). Results for alumina-based catalysts were compared with JCPDS file (Reference no. 98-001-3120). Similarly, Results for ceria-based catalysts were compared with JCPDS file (Reference no. 98-008-6411). The experimental error for the analysis was 0.01°.

The surface morphology and characteristics of chosen areas of samples were examined using the SEM (Nova Nano SEM 450) with an X-ray energy dispersive spectroscopy (EDS) system in order to identify the elements. The elemental composition was also identified through EDS mapping. The SEM pictures measurement indices ranged from 5 μm to 500 μm. To identify the surface and pore specifications, N_2 adsorption desorption at 77 K (liquid nitrogen temperature) is employed to analyze the textural qualities using the BET and BJH desorption techniques on (Meso 112) equipment. The surface area analysis and pore size distribution of catalysts was observed using BET surface analyzer. Prior to the analysis, the samples were vacuum degassed for two hours at 200 °C for the removal of adsorption species on the prepared sample.

4.3 Catalyst Testing

The catalyst activity was tested in a continuous tubular packed bed reactor of internal diameter 11.7 mm and length 60 cm. In all the experiment 0.769 gm of catalyst of size 180–300 micron was used. The catalyst was mixed with quartz particle of same size in 1 : 1 ratio. The L/dp ratio was maintained above 50 and D/dp ratio was maintained above 35 to overcome the mass transfer limitation. Initially, the catalyst was reduced for two hours at 850 °C temperature in the environment of 90 % N_2 and 10 % H_2 with a total flow of 110 ml/min. Thereafter, the reactor was flush with pure nitrogen for 1 hour to remove all the

hydrogen from the reactor and reactor was maintained at the desired operating temperature. Once the reactor temperature was maintained and no hydrogen was detected at the outlet of the reactor, methane, and water mixture was fed into the reactor along with nitrogen. The methane to steam ratio of 1 : 4 was maintained in all the experiments. The experiments were performed at a gas hourly space velocity (GHSV) of 10,739 hr^{-1} and W/F of 26.8 kg_{cat}. s/mol. The outlet gas passed through a condenser and gas-liquid separator to condense the liquid product The output gases were then analyzed with a TCD-equipped GC (Nucon GC) using a parallel column system of Porapak Q (1 m length, I.D 2 mm) and Molecular sieve (3 m length, I.D 2 mm). The following equations were used to calculate CH_4 conversion, CO selectivity, and CO_2 selectivity.

4.4 Results and Discussion

4.4.1 Characterization results

XRD

The XRD patterns show diffraction peaks for NiO and Al_2O_3. All metal-doping modifications and nickel-based catalysts share amorphous characteristics similar to Al_2O_3 as the metal loading is less (10 %). The XRD patterns of Ni, Ni-La, and Ni-Fe catalysts are shown in Fig 4.1. The diffraction peaks at 2θ: 42° and 48° identified the cubic NiO phase. Al_2O_3 is responsible for the peaks at 2θ: 2°, 38°, and 63°. The little shoulder associated with the NiO phase, centered at 2θ: 43°, becomes less noticeable with higher lanthanum loading. The lack of the lanthanum oxide phase shows that lanthanum is heavily scattered on the surface, which points to the presence of minute crystallites of lanthanum that are below the XRD detection threshold. This outcome is in line with observations made in the literature for a low percentage of La doping. [16,19] Martinez et al. [19] also reported the same observation for La/Al_2O_3 based catalysts at various La loading levels. The XRD

pattern of Fig 4.1 demonstrates the presence of peaks at 2θ: 38°, 42°, and 43° that correspond to the metallic phase.

XRD pattern of ceria supported catalysts is also shown in Fig 4.1. The ceria-based catalyst shows the crystalline phase for both the Ni-La/CeO_2 and Ni-Fe/ CeO_2 catalysts. Ni peaks are observed at 2θ: 47.5°, and 76.7°. The CeO_2 peaks are attributed at angle 2θ: 28.6°, 47.5°, 56.4°, and 69.4°. The Scherrer equation ($D = K\lambda/B\cos\Theta$) is used to analyze the XRD line broadening in order to determine the average crystallite size, where D is the mean crystal size, K is the dimensionless shape actor with a value of 0.9 by assuming spherical particles, λ is the X-ray wavelength, θ is Bragg angle and B is the line broadening at full width half the maximum intensity (FWHM). In a Ni-Fe/Al_2O_3 catalyst, the NiO crystallite size ranges from 5–7 nm. Whereas, the crystallite size of NiO in Ni-Fe/CeO_2 catalyst ranges from 21–23 nm. The difference in the crystallite sizes of NiO, demonstrates the nickel superior dispersion on the alumina based catalyst.

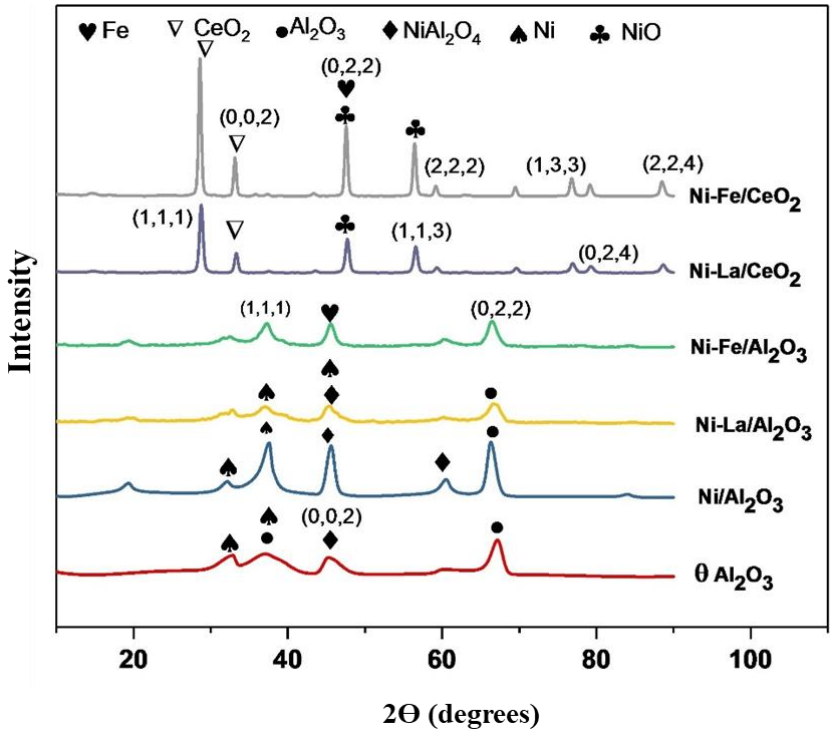

Fig. 4.1. XRD graph of La and Fe doped bimetallic catalysts

Similarly, the crystallite size of Ni-La/CeO_2 and Ni-La/Al_2O_3 is 18.168 nm and 6.456 nm respectively. However, Ni-La/Al_2O_3 crystallite size is the smallest which could be attributed to the high catalytic activity of Ni-La/ Al_2O_3 catalyst.

Table 4.1 shows the crystallite size of all the synthesized catalysts. The microstructural evidences gathered from XRD data is crystal size by matching the diffraction patterns within the material lattice that directly affect the reactivity of catalyst. Small crystal size sometimes responsible for the higher surface area of sample due to more no of active sites. Large crystal size leads to longer path for diffusion resulted into mass transfer limitations and reduced rate of reaction. This result is also confirmed by the BET results. The crystal structure and morphology can also influence reaction mechanism to increase/ decrease the CO selectivity.

BET

The BET surface area values for the prepared catalysts are summarized in Table 4.1. BET specific surface areas are measured by nitrogen adsorption desorption at 77 K (Meso 112 instrument). As Ni concentration rises, the BET surface area often declines due to pore blockage by the metal particles. Fig. 4.2, display the nitrogen adsorption-desorption isotherms of alumina and ceria supported catalysts respectively. Alumina supported catalysts show type 4 BET isotherm, while ceria supported catalysts follow type 3 isotherm. Table 4.1 also displays pore volume and pore diameter of all the prepared catalysts. The addition of La and Fe reduced the surface area and pore volume of catalyst which could be due to impregnation between smaller Ni particles. This alteration changes the surface characteristics of the catalysts on both the alumina and ceria support. A decrease in surface areas and pore volume after metal impregnation shows the substantial impact of La and Fe on the catalyst. The Ni-Fe/CeO_2 catalyst has a larger crystallite size of NiO (23.207 nm) as compared to Ni-Fe/Al_2O_3 catalyst (7.234 nm). The larger crystallites result in a lower

surface area of Ni-Fe/Al_2O_3 catalyst. The Ni-La/Al_2O_3 shows low crystallite size as compared to Ni-La/CeO_2. The catalyst with a higher surface area and smaller particle size shows better catalytic activity. So, it can be concluded that XRD and BET results are consistent.

Substituting nickel with lanthanum and iron lowers the pore diameter as shown in Table 4.2. After metal doping, pore diameter gets reduced because probe gas N_2 will not properly adsorb inside the pores due to blocking of pores. After the metal doping, some pore gets blocked. As promoters get into the pores therefore pore diameter gets reduced after metal doping. These metal particles can partially or totally block the pores as they group together and reduce the available pore diameter. Overall, the decrease in pore diameter observed after loading La and Fe onto a support material is due to a combination of variables such as pore filling, metal oxide formation, increased density, and metal particle aggregation. This result is in agreement with Boudjeloud et al. 2019,[16] Anekwe at al. 2024. [28] Therefore, with an increase in metal dopants, BET surface area also decreased. These results are also in agreement with Alipour et al. [18] For ceria-based catalysts, there is a formation of large NiO crystallites, due to that dispersion of Ni is lower in ceria-based catalysts as compared to alumina-based catalysts which can be attributed to the better catalytic activity of alumina catalysts for SMR. The increase in crystallite size leads to the agglomeration of particles and poor dispersion over the catalyst.

Table 4.2. BET surface area analysis of synthesized catalysts.

Catalyst	Surface Area (m^2/g) [a]	Pore Volume (cm^3/g) [b]	Pore Diameter (nm) [b]	Crystallite size (nm) [c]
γ-Alumina	235.7	0.464	7.75	17.24
θ-Alumina	134	0.243	6.941	15.289
Ni/Al_2O_3	106	0.194	6.296	13.375
$Ni\text{-}Fe/Al_2O_3$	99	0.144	5.822	7.234
$Ni\text{-}La/Al_2O_3$	102	0.164	5.945	6.456
CeO_2	19.2	0.045	9.369	26.12
Ni/CeO_2	12.3	0.030	6.773	24.54
$Ni\text{-}Fe/CeO_2$	4.3	0.007	6.627	23.207
$Ni\text{-}La/CeO_2$	9.7	0.017	7.143	18.168

[a] Measured by Brunauer-Emmett-Teller (BET) data. [b] Pore volume calculated by BJH desorption method. [c] Crystallite size of NiO calculated by Scherrer equation from XRD data.

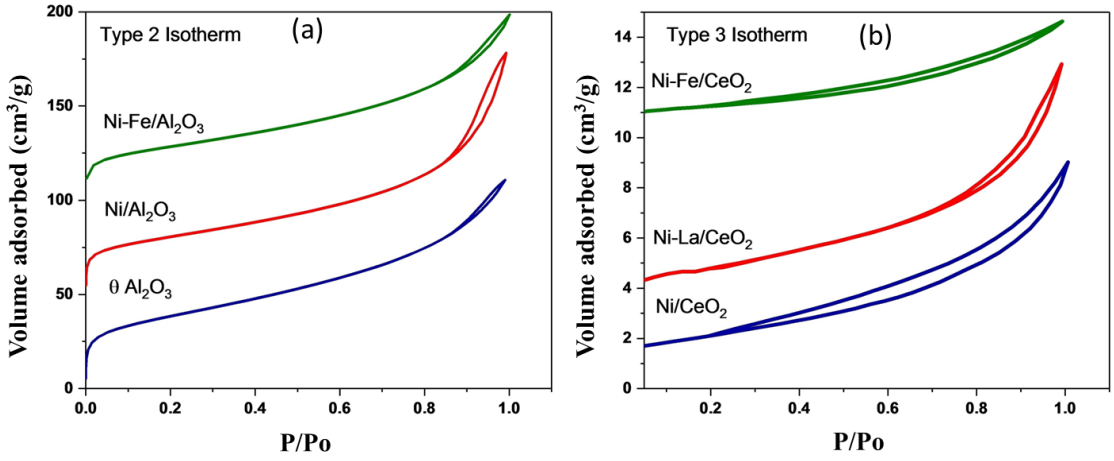

Fig. 4.2. BET Analysis of Ni/CeO_2, $Ni\text{-}La/CeO_2$, $Ni\text{-}Fe/CeO_2$.

SEM-EDS

Fig 4.3 a–f shows the SEM images of all the catalysts synthesized in the current work. The catalysts surface morphology is analyzed using scanning electron microscope (Nova Nano SEM 450) equipped with Energy dispersive spectroscopy (EDS) analyzer. To identify the elements that contribute to Ni/Al_2O_3 catalysts activity, SEM is employed to analyze the metal dispersion on the catalysts surface. There is no agglomeration of particles formed on the surface of catalysts. These catalysts are more resistant to coking because they don't produce the surface deposits of filamentous carbon that resemble whiskers, as depicted in Fig 4.3. Compared to Ni based monometallic catalysts with La and Fe promoted bimetallic catalysts showed small crystal size and good metal dispersion as observed by SEM images. Energy dispersive spectroscopy (EDS) is used to analyze the elemental composition of selected areas of the catalysts. EDS analysis is performed on the samples of $Ni\text{-}La/Al_2O_3$, and $Ni\text{-}La/CeO_2$ catalysts, as illustrated in Fig 4.4a and 4.4b respectively.

Table 4.3 displays the elemental compositions of all the synthesized catalysts. The total metal loading of the catalyst is 10 %. EDS results show uniform dispersion of all the metal across the catalyst surface and confirms the metal doping of Ni, La, Fe on the sample with appropriate composition.

Table 4.3. Elemental composition of catalysts through EDS analysis.

Catalyst	Ni (wt%)	La (wt %)	Fe (wt %)	Support (wt%)
Ni/Al_2O_3	11.81	–	–	88.19
$Ni\text{-}La/Al_2O_3$	8.35	2.62	–	89.03
$Ni\text{-}Fe/Al_2O_3$	7.39	–	2.54	90.07
Ni/CeO_2	10.78	–	–	89.22
$Ni\text{-}La/CeO_2$	8.15	3.45	–	88.4
$Ni\text{-}Fe/CeO_2$	7.18	–	2.52	90.3

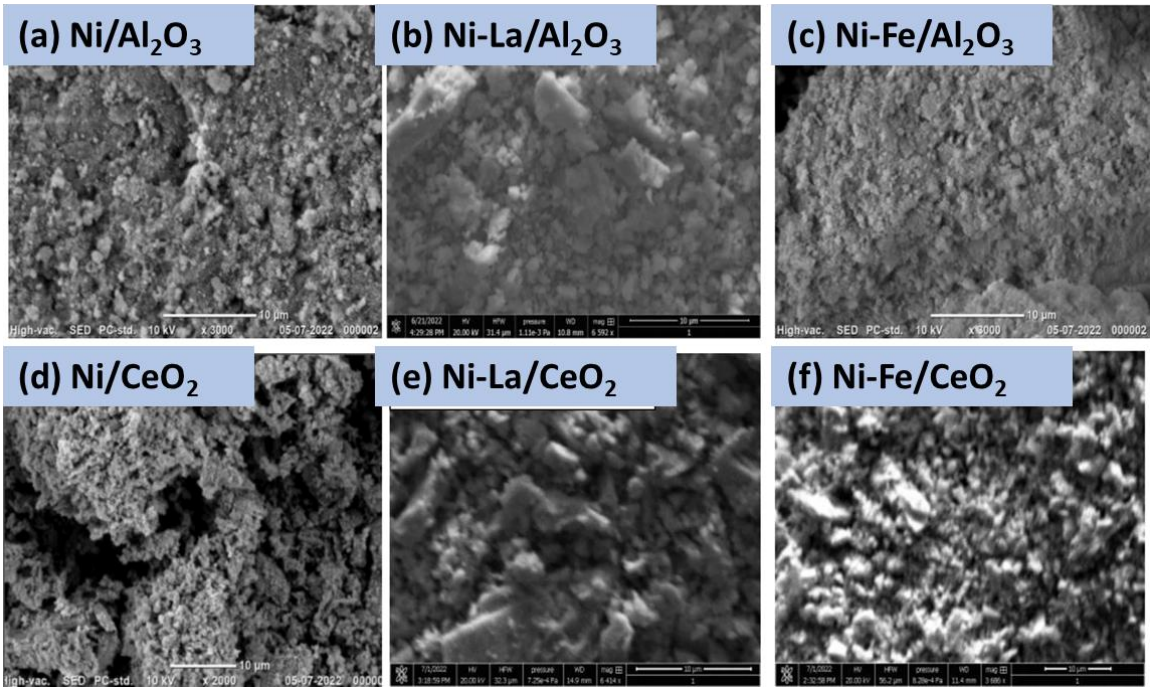

Fig. 4.3. SEM images of a) Ni/Al_2O_3, b) $Ni\text{-}La/Al_2O_3$, c) $Ni\text{-}Fe/Al_2O_3$, d) Ni/CeO_2, e) $Ni\text{-}La/CeO_2$, and f) $Ni\text{-}Fe/CeO_2$

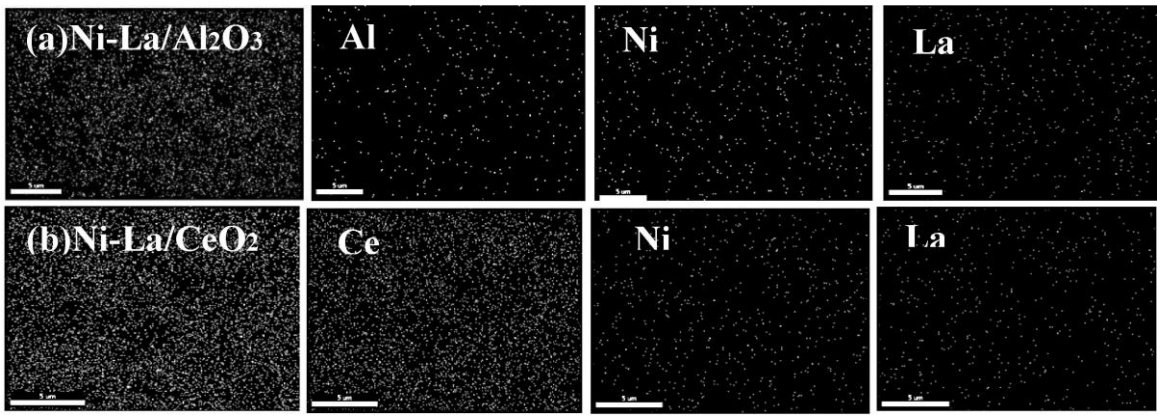

Fig. 4.4. a) EDS mapping of $Ni\text{-}La/Al_2O_3$, b) $Ni\text{-}La/CeO_2$.

4.4.2 Catalyst Activity Testing

The synthesized catalysts are tested in a packed bed reactor. Initially, the effect of the total flow rate is analyzed on catalytic activity to rule out any mass transfer limitation. In the region where the gas flow rate was higher than 70 ml/min, the rate of steam reforming was nearly constant, suggesting that the mass transfer effect is insignificant at and above this flow rate. Therefore, for all the experiments, the overall flow rate was maintained at 100

ml/min to ensure that the experiments were conducted within the zone of intrinsic kinetics. Further, the reactions on various average sizes of catalysts from (100-400 microns) are carried out. The methane conversion for the catalyst with particle sizes between 100 and 400 microns is found to be approximately the same, indicating that the intraparticle diffusion limitation is low in this range of operating conditions. As a result, the catalyst diameter is maintained throughout all studies between 180 and 300 microns.

The steam reforming of methane for all the synthesized catalysts is investigated in the temperature range of 500–800 °C at constant pressure (1 bar) in a packed bed reactor. The feed mixture consists of methane, steam, and nitrogen as the inert gas. For all the experiments steam to methane ratio is fixed at 4.0 and the weight of the catalyst to molar flow rate of methane (W/F) is maintained at 26.8 kg_{cat}.s/mol. It is investigated that how lanthanum and iron, as promoters with nickel, affect the catalytic activity of catalysts for both the alumina and ceria support at different temperatures. The performance of catalysts is analyzed in terms of methane conversion, CO, CO_2 selectivity and H_2 yield.

Methane Conversion

Fig 4.5a and 4.5b show the methane conversion for alumina and ceria-based catalysts respectively at different temperatures. The conversion of methane increases with an increase in temperature for all the catalysts (except Ni-Fe/CeO_2). The increase in conversion with temperature is rapid at lower temperatures compared to the higher temperature. The significant increase in CH_4 conversion observed between 550 to 650 °C may be attributed to a surface enrichment with a high Ni dispersion state in close contact with both La and Fe on both alumina and ceria-based supports. This demonstrates that another metal support interaction increases the CH_4 adsorption. Martinez et al. [19] also reported such type of interaction. Ni-La/Al_2O_3, tiny particle sizes promote relatively low temperature (500 °C) reaction, boosting CHx species dissociative adsorption on catalyst

surface and hence provides higher catalytic activity even at 500 °C temperatures. Iron catalysts supported on ceria were found to be ineffective for the methane decomposition reaction. The Ni-Fe/CeO_2 catalyst had less surface area, and its pore volume was also decreased (Table 4.1). The XRD analysis shows that the Ni-Fe alloy was formed on alumina support and remained stable during the reforming reaction. However, it did not form on the ceria-based support. On ceria support, the catalyst was found to be enriched in Ni species, whereas the Ni-Fe/Al_2O_3 catalyst was found to be enriched in Fe species which stimulates the water gas shift reaction.

The results show that La loading makes both alumina and ceria-based catalysts more active even at lower temperatures. This makes Ni-La catalyst supported on alumina and/or ceria suitable for 'on-site' hydrogen generation through a methane based membrane reformer. Ni-La/Al_2O_3 shows high conversion at low temperatures (50 % conversion at 500 °C) as compared to Ni-La/CeO_2 (20 % conversion at 500 °C). Another important parameter for membrane reformers is low start-up time (low response time of catalyst). Figs 4.6a, 4.6b, 4.6c, and 4.6d show the methane conversion with time for Ni-Fe/Al_2O_3, Ni-La/Al_2O_3, Ni-Fe/CeO_2, and Ni-La/CeO_2 catalysts respectively at different temperatures. The results show that for all the catalysts response time reduces with an increase in temperature i. e., the catalyst gives higher conversion in short time. However, Ni-La/Al_2O_3 and Ni-La/CeO_2 show low response time even at low temperature. Ni-La/Al_2O_3 catalyst shows 20 % conversion at 500 °C and 52 % conversion at 550 °C in 5 mins. Therefore, La is recommended to employ as a promoter instead of iron to lower the start-up time of the methane-based membrane reformer system. Additionally, adding lanthanum as a promoter increases the distance between the active nickel particles, inhibits particle aggregation, and reduces the sintering impact. [20] As per XRD data, lanthanum also contributes to reducing the nickel particle size which improves its dispersion. Ligthart et al. [20] reported that these

qualities work well to stop metal from sintering during the steam methane reforming reaction.

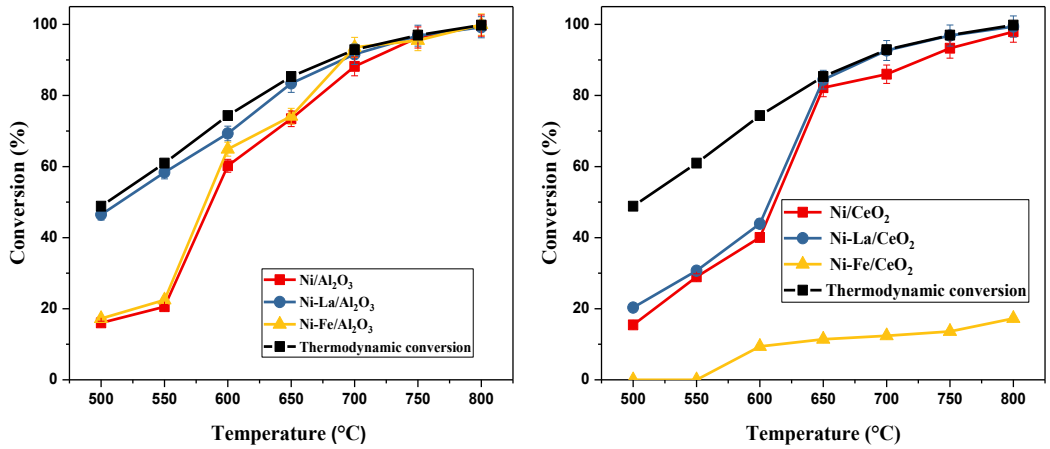

Fig. 4.5. Conversion vs temperature plots for a) Ni/Al_2O_3, $Ni\text{-}La/Al_2O_3$, $Ni\text{-}Fe/Al_2O_3$, b) Ni/CeO_2, $Ni\ La/CeO_2$, $Ni\ Fe/CeO_2$ (reaction conditions: P = 1 atm, $H_2O/\ CH_4$ = 4.0, W/F= 26.8 $Kg_{cat}.s/mol$)

CO and CO_2 Selectivity

Figs 4.7a and 4.7b show the CO selectivity of alumina and ceria based synthesized catalysts with temperature respectively. The CO selectivity is a vital parameter for membrane reformer when integrated with a proton exchange membrane fuel cell (PEMFC) to generate power. PEMFC requires low CO content (less than 5 ppm) and hence higher CO selective catalyst makes the membrane separation more critical. Further, the high CO content inhibits hydrogen permeation through palladium-based membranes (commonly used for hydrogen separation). There- fore, it is critical to have a catalyst that gives low CO selectivity for long term consistent performance of membrane reformer. The results show that CO selectivity increases with the temperature of all the catalysts. The water gas shift reaction is more active at low temperatures. Hence, at low temperatures it converts CO into CO_2 and reduces the CO selectivity, and increases the CO_2 selectivity (as shown in Fig 4.8a and 4.8b). In comparison to ceria supported catalysts, alumina supported catalysts show higher

CO selectivity. The oxygen storage abilities of ceria support enhance CO oxidation by mobilizing the lattice oxygen. Ce^{4+}/Ce^{3+} enables the formation of highly mobile oxygen species. This can be confirmed from the CO selectivity graph of ceria supported catalyst. Ni-La/CeO_2 shows lower CO selectivity as compared to Ni-La/Al_2O_3 due to formation of mobile oxygen species. The fluorite structure of CeO_2 allows for the formation of mobile oxygen with the reduction of Ce^{4+} to Ce^{3+}. This mobile oxygen combines with the CO molecule and increased the CO_2 selectivity which can be confirmed from the graph of CO_2 selectivity vs time (Fig 4.8). This data is also in agreement with Vecchietti et al., 2022. [29] They proved this with XPS and DFT calculations. This result is also in agreement with XPS and TPD experiments in Gunawan et al. 2019. [30]

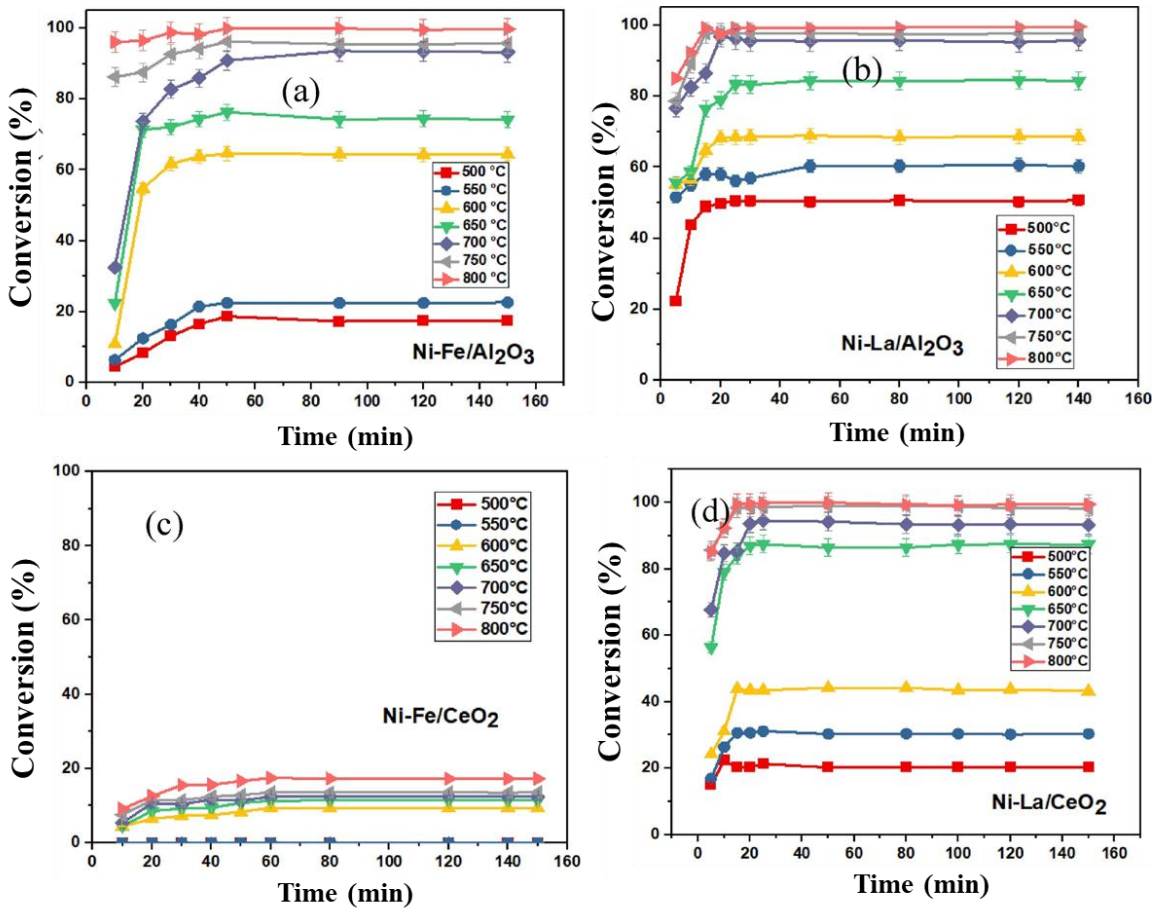

Fig. 4.6. Conversion vs time graph for a) Ni-Fe/Al_2O_3, b) Ni-La/Al_2O_3 c) Ni-Fe/CeO_2 d) Ni-La/CeO_2 catalysts at different temperatures.

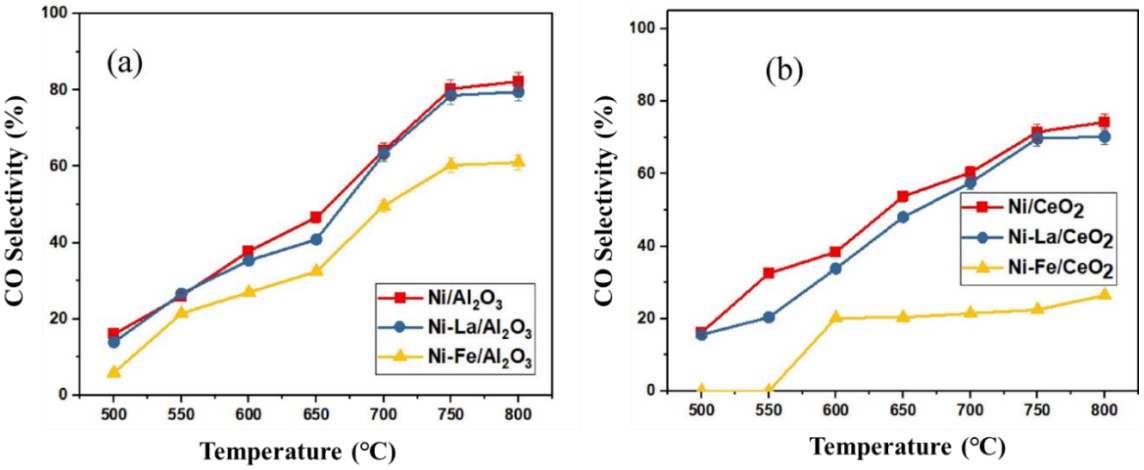

Fig. 4.7. CO selectivity with temperature for a) alumina supported b) ceria supported catalysts.

Strong interaction of nickel oxide and ceria was observed to exhibit higher catalytic activity. Further, water molecules are converted into active oxygen species at partially reduced ceria sites. Over Ni sites, methane is absorbed and forms Ni-C by removing hydrogen. The oxygen spillover from the support reacts with the carbonaceous molecules on the Ni sites and reduces carbon deposition on the catalyst support.

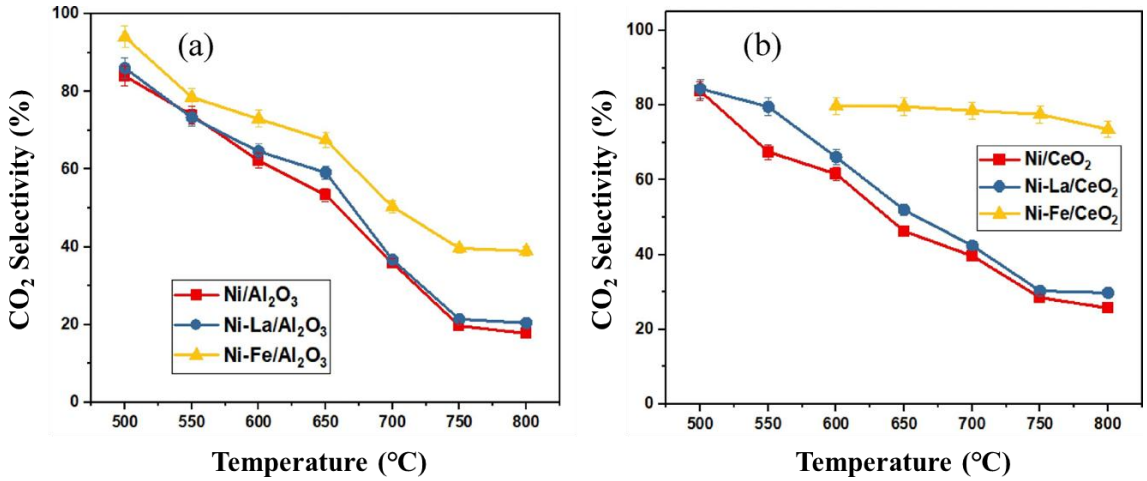

Fig. 4.8. CO_2 selectivity with temperature for a) alumina supported b) ceria supported catalysts.

Hence, ceria-based support shows low CO selectivity at all the temperature. At low temperatures (500–550 °C) alumina-based catalysts (Ni-La/Al_2O_3 and Ni-Fe/Al_2O_3) also show relatively low CO and high CO_2 selectivity. The CO selectivity at 500 °C for Ni-Fe/Al_2O_3 catalyst is 4 %. At low temperatures, Fe encourages the water gas shift reaction on an alumina-supported catalyst. Adding Fe to a Ni-Fe based catalyst also decreases the methanation reaction. [21] Further, FeO species in reduced catalysts may partially oxidize during the reforming process, which could reduce the CO selectivity by supplying the essential oxygen species. Ni-Fe alloy may also be oxidized by steam and helps in reducing the CO selectivity. La as a promoter has not much effect on CO or CO_2 selectivity. Hence, CO and CO_2 selectivity for Ni and Ni-La catalysts supported on alumina or ceria support have approximately the same selectivity for CO and CO_2. CO selectivity for Ni-Fe/CeO_2

catalyst is quite low (20 %) even at high temperature (750 °C). The oxygen storage capacity of both Fe and CeO_2 plays a vital role in reducing the CO selectivity and improving the CO_2 selectivity. Ni-Fe alloy formed on ceria support also get oxidized by excess steam and helps in reducing the CO selectivity for Ni-Fe/CeO_2 catalyst. However, the activity of Ni-Fe/CeO_2 catalyst is very low and hence it is not useful for membrane reformer application. Ni-Fe alloy formation is responsible for the increased CO_2 selectivity of the reaction. This Ni-Fe alloy formation is confirmed by the XRD data. The peak at 2Ɵ degree 47.34 also corresponds to Ni-Fe alloy formation. Where Ni-Fe alloy did not form on the ceria supported catalyst. Therefore, Ni-Fe catalyst is also not catalytically active on the ceria support. However, the Ni-Fe/Al_2O_3 catalyst was found to be enriched in Fe species which stimulates the water gas shift reaction and increased the CO_2 selectivity with the alumina support. As part of their catalytic cycle, iron-based catalysts have the capacity to both store and release oxygen species. These oxygen species have the ability to adsorb and desorb oxygen to and from the catalyst surface in processes like oxidation-reduction cycles. The water-gas shift (WGS) reaction, which changes carbon monoxide (CO) into carbon dioxide (CO_2) and lowers CO selectivity, can be aided by the presence of oxygen species. These results are in agreement with chang et al. 2020. [31] They explained this using XPS analysis. Ni-La supported on CeO_2/Al_2O_3 show high catalytic activity (conversion) and low CO selectivity at low temperature which makes them suitable for membrane reformer application. However, ceria supported Ni-La catalyst is more active after 600 °C temperature.

4.5 Cobalt based bimetallic catalysts:

The graph compares the performance of various catalysts in steam methane reforming, with the two plots representing catalysts supported on Al_2O_3 and CeO_2.

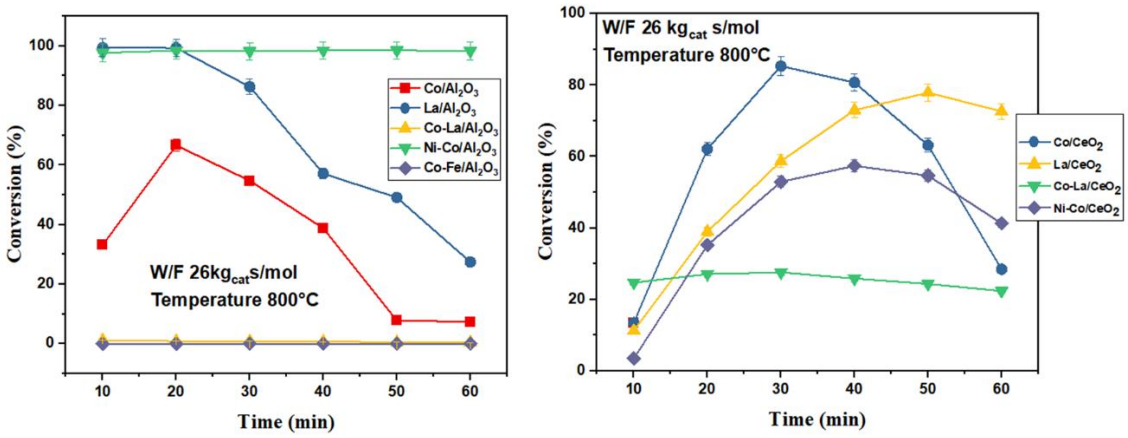

Fig. 4.9. Conversion vs time graph of (a) alumina supported catalysts (b) ceria supported catalysts

4.5.1 Alumina Supports

Fig 4.9(a) shows the activity trends of catalysts supported on Al_2O_3. Among these, the Ni-Co/Al_2O_3 catalyst exhibits constant and high activity, maintaining nearly 100% methane conversion across all temperatures. [32-36] La/Al_2O_3 shows moderate activity but decreases as the time rises. Meanwhile, Co/Al_2O_3 shows low activity overall, peaking at mid-temperatures and dropping significantly at higher time. The other catalysts, Co-La/Al_2O_3 and Co-Fe/Al_2O_3, exhibit minimal to no activity, as indicated by their near-zero conversion throughout the reaction time. [37]

4.5.2 Cerium Oxide

In Fig 4.9(b), catalysts supported on CeO_2 display better performance compared to Al_2O_3 supported catalysts. La/CeO_2 and Co/CeO_2 exhibit higher conversion values, peaking at mid-reaction time, with La/CeO_2 maintaining relatively high activity throughout. [38-42]

Ni-Co/CeO_2 also shows moderate conversion but starts lower compared to the others. In contrast, the Co-La/CeO_2 catalyst maintains a consistent, low activity, similar to Ni-Co/Al_2O_3. The results highlight the significant impact of the support material on catalyst performance in steam methane reforming. CeO_2 supported catalysts demonstrate higher activity and stability compared to their Al_2O_3 counterparts. Among all, Ni-Co/Al_2O_3 shows exceptional stability, while La/CeO_2 and Co/CeO_2 achieve the best performance on ceria supports.

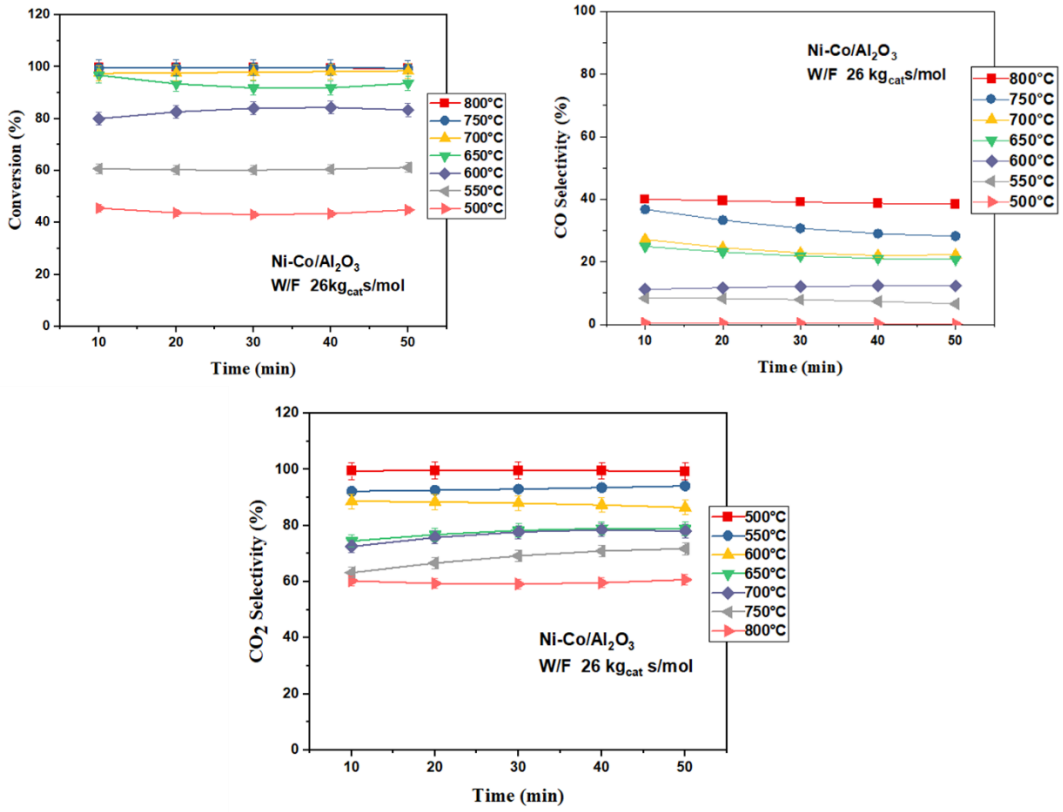

Fig. 4.10. Catalyst activity of Ni-Co/Al_2O_3 catalyst (a) Methane conversion vs time (b) CO selectivity vs time (c) CO_2 selectivity vs time graph

The graph Fig 4.10 illustrates the performance of catalysts in steam methane reforming by plotting methane conversion, CO selectivity, and CO_2 selectivity against time-on-stream at different temperatures (500°C to 800°C). [43-46] In Fig 4.10(a) (methane conversion vs.

time), methane conversion increases with temperature. At 800°C and 750°C, the conversion remains consistently high, indicating excellent catalytic activity. However, as the temperature decreases (e.g., 650°C and below), conversion drops significantly, especially at 500°C, where the catalysts exhibit minimal activity. Catalyst performance at higher temperatures demonstrates its strong thermal activation, enabling efficient methane reforming. The Fig 4.10(b) (CO selectivity vs. time) shows the CO production trend at various temperatures. At high temperatures (800°C and 750°C), CO selectivity is dominant and stable, reflecting the promotion of the reverse water-gas shift reaction, which favors CO formation over CO_2. [47-50] At lower temperatures (below 650°C), CO selectivity decreases, suggesting less efficient methane cracking and reforming.

In Fig 4.10(c) (CO_2 selectivity vs. time), CO_2 selectivity exhibits an inverse trend compared to CO selectivity. At lower temperatures (500°C to 650°C), CO_2 production is higher, indicating that the water-gas shift reaction is more favorable under these conditions. However, as the temperature rises (750°C and 800°C), CO_2 selectivity decreases, while CO selectivity increases, showing the competitive nature of the reactions at higher temperatures.

At high temperatures (800°C, 750°C), the catalysts achieve high methane conversion with dominant CO selectivity, while CO_2 selectivity is suppressed. At lower temperatures, methane conversion decreases, CO selectivity drops, and CO_2 selectivity increases, indicating a shift in reaction pathways. This analysis highlights the importance of temperature in determining catalytic efficiency and product distribution during steam methane reforming. [51-52]

4.6 Conclusions

For steam reforming of methane, the catalytic efficiency of six Ni based catalysts was evaluated on alumina and ceria support for ‘on-site’ generation of hydrogen through

membrane reformer. Experiments were performed at different temperatures and 1 bar pressure for steam to methane ratio of 4.0 and W/F 26.8 kg_{cat}.s/mol. The effect of La and Fe was observed on both alumina and ceria supports. It was found that Fe as a promoter enhances the oxygen storage capacity for both ceria and alumina-based Ni catalysts. This helped in reducing the CO selectivity and enhancing the CO_2 selectivity of Fe promoted catalysts. However, hydrogen yield and methane conversion were low for Fe promoted catalysts. La promoted catalysts show high catalytic activity for both alumina and ceria supported Ni-based catalysts. The high oxygen vacancies of La enhance the H2O adsorption on catalysts surface. The enhanced H_2O adsorption promotes carbon gasification and water gas shift reaction. The high oxygen vacancies of La and Fe both enhanced the H_2O adsorption on catalysts surface. It can be directly confirmed with CO_2 selectivity of graph. (Fig 9) Where it can be seen that both La and Fe promoted the water gas shift reaction by enhancing the H_2O adsorption over the surface of catalyst. Lanthanum also reported to lower the startup time of the reaction as the rate of adsorption of H_2O is faster as compared to Fe as promoter. Because oxygen vacancies provide active sites for oxygen adsorption and absorption into the catalyst lattice, they facilitate the production of surface hydroxyl groups (OH-). Through their ability to facilitate intermediate species adsorption and promote reaction path-ways, surface hydroxyl groups are essential in a variety of catalytic reactions, including the steam methane reforming process.

This resulted in high methane conversion and high hydro- gen yield. La promoted catalyst also reduced the size of Ni particles and hence provided more active sites. The smaller Ni particle amplified the dissociative adsorption of CH_4, resulting in increased catalytic activity. Further, La also widens the distance between Ni particles and prevents agglomeration which increases the stability of the catalysts. The La promoted catalysts also provided low start-up time which is a critical parameter for on-site hydrogen generation

through membrane reformer. Hence, La promoted Ni-based catalyst supported on alumina and ceria support would be the preferred choice. However, Ni-La/Al_2O_3 provided higher conversion at low temperatures. It also gave low CO selectivity and higher hydrogen yield at lower temperatures (500–550 °C). These qualities made it a suitable catalyst amongst the investigated catalysts for membrane reformer application. Ni-Co bimetallic combination also shows high conversion as compared to other cobalt bimetallic catalysts but this catalyst is deactivating after 12 hours of study. Overall, Ni-La, Ni-Fe and Ni-Co bimetallic combinations shows high catalytic activity with low CO selectivity. This can be concluded that trimetallic catalysts with these combinations can even provide high conversion with zero CO selectivity. In literature, several catalysts are proposed for steam methane reforming which performs in the range of 600-800 °C. However, all of these catalysts show high CO selectivity at higher temperature and low conversion at low temperature. In chapter 5, various combinations of trimetallic catalysts of Ni, Fe, La, and Co on alumina support is prepared using wet impregnation method to obtained maximum conversion at low temperature and to promote water gas shift reaction. The synthesized catalysts are tested in a packed bed reactor (ID 11.74 mm) for different temperatures (500-800°C). A complete characterization of the catalyst is performed using Brunauer Teller Emmett (BET), X-ray Diffraction (XRD), Field Emission Scanning Electron microscopy (FESEM), Energy dispersive X-ray (EDX), X-ray photoelectron spectroscopy (XPS), Fourier transform infrared spectroscopy (FTIR), (Transmission electron microscopy) TEM.

References

1. Amjad, U. E. S., Vita, A., Galletti, C., Pino, L., Specchia, S. (2013). Comparative study on steam and oxidative steam reforming of methane with noble metal catalysts. *Industrial & Engineering Chemistry Research*, 52(44), 15428-15436.
2. Luna, E. C., Becerra, A. M., Dimitrijewits, M. I. (1999). Methane steam reforming over rhodium promoted Ni/Al_2O_3 catalysts. *Reaction Kinetics and Catalysis Letters*, 67, 247-252.
3. Halabi, M. H., De Croon, M. H. J. M., Van der Schaaf, J., Cobden, P. D., Schouten, J. C. (2010). Low temperature catalytic methane steam reforming over ceria–zirconia supported rhodium. *Applied Catalysis A: General*, 389(1-2), 68-79.
4. Wolf, M. (2021). Thermodynamic assessment of the stability of bulk and nanoparticulate cobalt and nickel during dry and steam reforming of methane. *RSC advances*, 11(30), 18187-18197.
5. Foletto, E. L., Alves, R. W., Jahn, S. L. (2006). Preparation of Ni/Pt catalysts supported on spinel ($MgAl_2O_4$) for methane reforming. *Journal of power sources*, 161(1), 531-534.
6. Gao, Q. Y., Lv, G. X., Mol, J. (2008). Effect of Pt and Pd on the dispersion of Ni particles and coking resistance for nickel based catalysts. *Catal Chin*, 22, 294-301.
7. Uemiya, S., Sato, N., Ando, H., Matsuda, T., Kikuchi, E. (1990). Steam reforming of methane in a hydrogen-permeable membrane reactor. *Applied catalysis*, 67(1), 223-230.
8. Shu, J., Grandjean, B. P. A., Kaliaguine, S. (1995). Asymmetric Pd-Ag/stainless steel catalytic membranes for methane steam reforming. *Catalysis today*, 25(3-4), 327-332.
9. Hashemnejad, S. M., Parvari, M. (2011). Deactivation and regeneration of nickel-based catalysts for steam-methane reforming. *Chinese Journal of catalysis*, 32(1-2),

273-279.

10. Lertwittayanon, K., Atong, D., Aungkavattana, P., Wasanapiarnpong, T., Wada, S., Sricharoenchaikul, V. (2010). Effect of $CaO–ZrO_2$ addition to Ni supported on γ-Al_2O_3 by sequential impregnation in steam methane reforming. *International journal of hydrogen energy*, 35(22), 12277-12285.
11. Abdelsadek, Z., Köten, H., Gonzalez-Cortes, S., Cherifi, O., Halliche, D., Masset, P. J. (2023). Lanthanum-promoted nickel-based catalysts for the dry reforming of methane at low temperatures. *Jom*, 75(3), 727-738.
12. Lucrédio, A. F., Jerkiewickz, G., Assaf, E. M. (2007). Nickel catalysts promoted with cerium and lanthanum to reduce carbon formation in partial oxidation of methane reactions. *Applied Catalysis A: General*, 333(1), 90-95.
13. Liu, B. S., Au, C. T. (2003). Carbon deposition and catalyst stability over La_2NiO_4/γ-Al_2O_3 during CO_2 reforming of methane to syngas. *Applied Catalysis A: General*, 244(1), 181-195.
14. Al-Fatesh, A. S., Naeem, M. A., Fakeeha, A. H., Abasaeed, A. E. (2014). Role of La_2O_3 as promoter and support in Ni/γ-Al_2O_3 catalysts for dry reforming of methane. *Chinese Journal of Chemical Engineering*, 22(1), 28-37.
15. Kobayashi, Y., Horiguchi, J., Kobayashi, S., Yamazaki, Y., Omata, K., Nagao, D.,Yamada, M. (2011). Effect of NiO content in mesoporous NiO–Al_2O_3 catalysts for high pressure partial oxidation of methane to syngas. *Applied Catalysis A: General*, 395(1-2), 129-137.
16. Boudjeloud, M., Boulahouache, A., Rabia, C., Salhi, N. (2019). La-doped supported Ni catalysts for steam reforming of methane. *International journal of hydrogen energy*, 44(20), 9906-9913.
17. Sharma, R., Kumar, A., Upadhyay, R. K. (2019). Bimetallic Fe promoted catalyst for

CO free hydrogen production in high temperature methanol steam reforming. *ChemCatChem*, 11(18), 4568-4580.

18. Alipour, Z., Borugadda, V. B., Wang, H., Dalai, A. K. (2022). Dry reforming of methane and biogas to produce syngas: a review of catalysts and process conditions. *Carbon Dioxide Capture and Conversion*, 201-235.
19. Martınez, R., Romero, E., Guimon, C.,Bilbao, R. (2004). CO_2 reforming of methane over coprecipitated Ni-Al catalysts modified with lanthanum. *Applied Catalysis A: General*, 274(1-2), 139-149.
20. Ligthart, D. M., Pieterse, J. A., Hensen, E. J. (2011). The role of promoters for Ni catalysts in low temperature (membrane) steam methane reforming. *Applied Catalysis A: General*, 405(1-2), 108-119.
21. Abelló, S., Bolshak, E., Montane, D. (2013). Ni–Fe catalysts derived from hydrotalcite-like precursors for hydrogen production by ethanol steam reforming. *Applied Catalysis A: General*, 450, 261-274.
22. Tomishige, K., Li, D., Tamura, M., Nakagawa, Y. (2017). Nickel–iron alloy catalysts for reforming of hydrocarbons: preparation, structure, and catalytic properties. *Catalysis Science & Technology*, 7(18), 3952-3979.
23. Angeli, S. D., Turchetti, L., Monteleone, G., Lemonidou, A. A. (2016). Catalyst development for steam reforming of methane and model biogas at low temperature. *Applied Catalysis B: Environmental*, 181, 34-46.
24. Fang, X., Zhang, X., Guo, Y., Chen, M., Liu, W., Xu, X., Li, C. (2016). Highly active and stable Ni/$Y_2Zr_2O_7$ catalysts for methane steam reforming: On the nature and effective preparation method of the pyrochlore support. *International journal of hydrogen energy*, 41(26), 11141-11153.
25. Zhai, X., Ding, S., Liu, Z., Jin, Y.,Cheng, Y. (2011). Catalytic performance of Ni

catalysts for steam reforming of methane at high space velocity. *International journal of hydrogen energy*, 36(1), 482-489.

26. Sharma, P. O., Abraham, M. A., Chattopadhyay, S. (2007). Development of a novel metal monolith catalyst for natural gas steam reforming. *Industrial & engineering chemistry research*, 46(26), 9053-9060.
27. Roh, H. S., Lee, D. K., Koo, K. Y., Jung, U. H., Yoon, W. L. (2010). Natural gas steam reforming for hydrogen production over metal monolith catalyst with efficient heat-transfer. *International journal of hydrogen energy*, 35(4), 1613-1619.
28. Anekwe, I. M. S., Oboirien, B., Isa, Y. M. (2024). Effects of transition metal doping on the properties and catalytic performance of ZSM-5 zeolite catalyst on ethanol-to-hydrocarbons conversion. *Fuel Communications*, 18, 100101.
29. Vecchietti, J., Pérez-Bailac, P., Lustemberg, P. G., Fornero, E. L., Pascual, L., Bosco, M. V., Bonivardi, A. L. (2022). Shape-controlled pathways in the hydrogen production from ethanol steam reforming over ceria nanoparticles. *ACS catalysis*, 12(16), 10482-10498.
30. Gunawan, C., Lord, M. S., Lovell, E., Wong, R. J., Jung, M. S., Oscar, D., Amal, R. (2019). Oxygen-vacancy engineering of cerium-oxide nanoparticles for antioxidant activity. *ACS omega*, 4(5), 9473-9479.
31. Chang, H., Bjørgum, E., Mihai, O., Yang, J., Lein, H. L., Grande, T., Chen, D. (2020). Effects of oxygen mobility in La-Fe based perovskites on the catalytic activity and selectivity of methane oxidation. *ACS Catalysis*, 10(6), 3707-3719.
32. Etminan, A., Sadrnezhaad, S. K. (2022). A two step Microwave-assisted coke resistant mesoporous Ni-Co catalyst for methane steam reforming. *Fuel*, 317, 122411.
33. You, X., Wang, X., Ma, Y., Liu, J., Liu, W., Xu, X., Chen, X. (2014). Ni–Co/ Al_2O_3 bimetallic catalysts for CH_4 steam reforming: elucidating the role of Co for improving

coke resistance. *ChemCatChem*, 6(12), 3377-3386.

34. Braga, A. H., de Oliveira, D. C., Taschin, A. R., Santos, J. B., Gallo, J. M. R., C. Bueno, J. M. (2021). Steam reforming of ethanol using Ni-Co catalysts supported on $MgAl_2O_4$ structural study and catalytic properties at different temperatures. *ACS Catalysis*, 11(4), 2047-2061.
35. Hu, X., Lu, G. (2007). Investigation of steam reforming of acetic acid to hydrogen over Ni–Co metal catalyst. *Journal of Molecular Catalysis A: Chemical*, 261(1), 43-48.
36. Zolghadri, S., Honarvar, B., Rahimpour, M. R. (2023). Synthesis, application, and characteristics of mesoporous alumina as a support of promoted Ni-Co bimetallic catalysts in steam reforming of methane. *Fuel*, 335, 127005.
37. Aunmunkong, P., Chaisuk, C. (2022). The Ni Catalyst Supported on the FSP-made Transition Metal (Co, Mn, Cu or Zn) Doped La_2O_3 Material for the Dry Reforming of Methane. *Bulletin of Chemical Reaction Engineering & Catalysis*, 17(1), 88-102.
38. Pino, L., Vita, A., Cipitì, F., Laganà, M., Recupero, V. (2011). Hydrogen production by methane tri-reforming process over Ni ceria catalysts: Effect of La-doping. *Applied Catalysis B: Environmental*, 104(1-2), 64-73.
39. Greluk, M., Rotko, M., Turczyniak-Surdacka, S. (2020). Enhanced catalytic performance of La_2O_3 promoted Co/CeO_2 and Ni/CeO_2 catalysts for effective hydrogen production by ethanol steam reforming. *Renewable Energy*, 155, 378-395.
40. Liu, F., Zhao, L., Wang, H., Bai, X., Liu, Y. (2014). Study on the preparation of Ni-La-Ce oxide catalyst for steam reforming of ethanol. *International journal of hydrogen energy*, 39(20), 10454-10466.
41. Zhao, J., Xu, X., Zhou, W., Blakey, I., Liu, S., Zhu, Z. (2017). Proton-conducting La-doped ceria-based internal reforming layer for direct methane solid oxide fuel cells. *ACS applied materials & interfaces*, 9(39), 33758-33765.

42. Calles, J. A., Carrero, A., Vizcaíno, A. J. (2009). Ce and La modification of mesoporous Cu–Ni/SBA-15 catalysts for hydrogen production through ethanol steam reforming. *Microporous and mesoporous materials*, 119(1-3), 200-207.

43. Ay, H., Üner, D. (2015). Dry reforming of methane over CeO_2 supported Ni, Co and Ni–Co catalysts. *Applied Catalysis B: Environmental*, 179, 128-138.

44. Nabgan, W., Abdullah, T. A. T., Mat, R., Nabgan, B., Triwahyono, S., Ripin, A. (2016). Hydrogen production from catalytic steam reforming of phenol with bimetallic nickel-cobalt catalyst on various supports. *Applied Catalysis A: General*, 527, 161-170.

45. Busca, G., Costantino, U., Montanari, T., Ramis, G., Resini, C., Sisani, M. (2010). Nickel versus cobalt catalysts for hydrogen production by ethanol steam reforming: Ni-Co-Zn-Al catalysts from hydrotalcite-like precursors. *International journal of hydrogen energy*, 35(11), 5356-5366.

46. He, L., Berntsen, H., Ochoa-Fernández, E., Walmsley, J. C., Blekkan, E. A., Chen, D. (2009). Co-Ni catalysts derived from hydrotalcite-like materials for hydrogen production by ethanol steam reforming. *Topics in Catalysis*, 52, 206-217.

47. Papageridis, K. N., Siakavelas, G., Charisiou, N. D., Avraam, D. G., Tzounis, L., Kousi, K., Goula, M. A. (2016). Comparative study of Ni, Co, Cu supported on γ-alumina catalysts for hydrogen production via the glycerol steam reforming reaction. *Fuel Processing Technology*, 152, 156-175.

48. Shi, K., An, X., Wu, X., Xie, X. (2022). Modification strategies for enhancing anti-coking of Ni-, Co-based catalysts during ethanol steam reforming: A review. *International Journal of Hydrogen Energy*, 47(93), 39404-39428.

49. Horlyck, J., Lawrey, C., Lovell, E. C., Amal, R., Scott, J. (2018). Elucidating the impact of Ni and Co loading on the selectivity of bimetallic Ni Co catalysts for dry

reforming of methane. *Chemical Engineering Journal,* 352, 572-580.

50. Papalas, T., Antzaras, A. N., Lemonidou, A. A. (2024). Unravelling the role of Co in mixed Ni-Co oxygen carriers/catalysts for H_2 production via sorption enhanced steam methane reforming coupled with chemical looping. *Applied Catalysis B: Environment and Energy*, 347, 123777.
51. Pinton, N., Vidal, M. V., Signoretto, M., Martínez-Arias, A., Corberán, V. C. (2017). Ethanol steam reforming on nanostructured catalysts of Ni, Co and CeO_2: Influence of synthesis method on activity, deactivation and regenerability. *Catalysis Today*, 296, 135-143.
52. Xu, J., Zhou, W., Li, Z., Wang, J., Ma, J. (2010). Biogas reforming for hydrogen production over a Ni–Co bimetallic catalyst: effect of operating conditions. *International Journal of Hydrogen Energy*, 35(23), 13013-13020.